

Geophysical Research Letters®

RESEARCH LETTER

10.1029/2022GL100120

Key Points:

- Meteorological conditions contributed significantly to atmospheric mercury seasonality across diverse temperate regions particularly Asia
- Typical monsoon climate in Asia led to differences in the crucial meteorological factors between Asia and other temperate regions
- Significant contributions of meteorological factors predicted further changes in atmospheric mercury seasonality under future global warming

Supporting Information:

Supporting Information may be found in the online version of this article.

Correspondence to:

L. Chen,
chenlong@geo.ecnu.edu.cn

Citation:




Xu, Z., Chen, L., Zhang, Y., Han, G., Chen, Q., Chu, Z., et al. (2022). Meteorological drivers of atmospheric mercury seasonality in the temperate Northern Hemisphere. *Geophysical Research Letters*, 49, e2022GL100120. <https://doi.org/10.1029/2022GL100120>

Received 20 JUN 2022

Accepted 4 OCT 2022

© 2022. American Geophysical Union.
All Rights Reserved.

Meteorological Drivers of Atmospheric Mercury Seasonality in the Temperate Northern Hemisphere

Zeng Xu¹, Long Chen^{1,2} , Yanxu Zhang³ , Guoling Han¹, Qing Chen¹, Zhaohan Chu⁴, Yanping Zhang¹, Chao Li^{1,2} , Yi Yang^{1,2}, and Xuejun Wang⁴

¹Key Laboratory of Geographic Information Science (Ministry of Education), School of Geographic Sciences, East China Normal University, Shanghai, China, ²Key Laboratory of Spatial-temporal Big Data Analysis and Application of Natural Resources in Megacities, Ministry of Natural Resources, Shanghai, China, ³School of Atmospheric Sciences, Nanjing University, Nanjing, China, ⁴Ministry of Education Laboratory of Earth Surface Process, College of Urban and Environmental Sciences, Peking University, Beijing, China

Abstract Mercury (Hg) is a neurotoxic pollutant that can be transported globally by atmospheric circulation and poses risks to wildlife and humans. Strong atmospheric Hg seasonality has been observed in the temperate Northern Hemisphere and explained by several hypothetical mechanisms. Here, we found that meteorological conditions were important drivers of the seasonality across diverse temperate regions particularly Asia through various indirect effects. Meteorological conditions can explain approximately 47%, 43%, and 67% of the seasonal amplitudes at the North American (NA) remote sites, European remote sites, and Asian monsoon sites, respectively. Surface air temperature, solar radiation, and surface wind collectively contributed significantly to the seasonality at the NA and European sites through vegetation resistance and oceanic evasion, while monsoon wind and precipitation promoted the summertime removal of Hg at the Asian sites through atmospheric transport and wet deposition, respectively. The findings predicted further changes in atmospheric Hg seasonality under future global warming.

Plain Language Summary Mercury is a neurotoxic pollutant that can be transported globally by atmospheric circulation before being removed from the atmosphere by deposition. Deposited mercury poses potential risks to ecosystems and human health owing to methylation and bioaccumulation. Strong seasonality of atmospheric mercury concentrations has been observed in the temperate Northern Hemisphere. Several hypotheses have been proposed to explain this strong seasonality, including vegetation uptake, chemical transformations, and anthropogenic emissions. In this study, we found that meteorological conditions were important drivers of the seasonality across diverse temperate regions particularly Asia through various indirect effects. Typical monsoon climate in Asia led to differences in the crucial meteorological factors between Asia and other temperate regions.

1. Introduction

Mercury (Hg) is a neurotoxic pollutant ubiquitously present in the environment (Obrist et al., 2021). Atmospheric Hg cycling is a crucial component of biogeochemical Hg cycling, owing to the extreme volatility of Hg (Sommar et al., 2020). Atmospheric Hg consists of a gaseous, elemental, and dominant type (Hg⁰; approximately 95%), and a gaseous or particulate divalent type (Hg^{II}) (Lindberg & Stratton, 1998). Owing to its low chemical reactivity and water solubility, Hg⁰ has a long lifespan in the troposphere (0.8–1.3 a) (Saiz-Lopez et al., 2018). It can be transported globally through atmospheric circulation before being adsorbed by vegetation and soils through dry deposition (Gustin et al., 2008; Wright et al., 2016) or transformed into Hg^{II}, which is easily removed by wet deposition (Lyman et al., 2020). Deposited Hg potentially poses risks to wildlife and humans owing to its methylation and bioaccumulation characteristics (Roman et al., 2011; Zhang et al., 2010, 2021).

Seasonality of atmospheric Hg concentrations has been observed at multiple ground-based monitoring sites worldwide. In particular, the observed seasonality is stronger in the temperate Northern Hemisphere, which includes forest, coastal, and urban sites (Fu et al., 2019; Sprovieri et al., 2016; Weigelt et al., 2015). For instance, atmospheric Hg concentrations in summer accounted for 94% of those in winter at all sites from Canadian Atmospheric Mercury Network during 1995–2005 (Temme et al., 2007). The seasonal amplitudes of atmospheric Hg

concentrations at five temperate Northern Hemisphere sites averaged 0.39 ng m^{-3} , equaling 25% of the background concentrations in the hemisphere ($1.5\text{--}1.7 \text{ ng m}^{-3}$) (Jiskra et al., 2018; Sprovieri et al., 2016).

Atmospheric Hg cycling is controlled by various atmospheric processes such as emissions, chemical transformations, atmospheric transport, dry deposition, and wet deposition. Accordingly, several hypothetical mechanisms based on these processes have been proposed to explain the strong seasonality in the temperate Northern Hemisphere, including vegetation uptake, chemical transformations, natural emissions, and anthropogenic emissions (Fu et al., 2015; Holmes et al., 2010; Horowitz et al., 2017; Jiskra et al., 2018). For instance, evidence of both Hg stable isotope signatures in litterfall (Liu et al., 2021; Wang, Bao, et al., 2016, 2020b) and the consistent seasonality between atmospheric Hg concentrations and vegetation activity (Jiskra et al., 2018) have confirmed the control of vegetation uptake on atmospheric Hg seasonality in the temperate Northern Hemisphere (MacSween, Edwards, & Beggs, 2020; Yu et al., 2018; Zhou et al., 2021). Additionally, high oxidant concentrations (e.g., Br, NO_2 , and HO_2 radicals) during warm months contribute to the high transformation rate of Hg^0 to Hg^{II} and its subsequent removal via Hg^{II} deposition (Obrist et al., 2011; Pal & Ariya, 2004). Significant anthropogenic emissions from coal combustion occur during cold months owing to increased energy demands for heating, leading to elevated atmospheric Hg concentrations during this period (Liu et al., 2019; Wang et al., 2018; Weigelt et al., 2015).

Meteorological conditions have been recognized as key drivers that can induce seasonal variations of the atmospheric processes and subsequently induce atmospheric Hg seasonality indirectly. For instance, frequent rain and strong prevailing wind can contribute to the removal of atmospheric Hg through vertical wet deposition and horizontal atmospheric transport, respectively (Horowitz et al., 2017; Koenig et al., 2021; Sprovieri et al., 2017; Wang, Wang, & Zhang, 2020). Factors such as solar radiation, surface wind, and temperature can affect the natural emissions of Hg from the soil, snow, and ocean (Aspmo et al., 2006; Carbone et al., 2016; MacSween, Edwards, & Beggs, 2020). Although the role of meteorological conditions has previously been proposed (Fu et al., 2015; Liu et al., 2016; Tseng et al., 2012), their contributions to hemispherical seasonality have not been quantified, and the identification of crucial meteorological factors and the atmospheric processes of relevance have been poorly understood. This is in contrast to both the understanding of the driving forces of atmospheric Hg seasonality and projections of changes in biogeochemical Hg cycles under future climate change (Krabbenhoft & Sunderland, 2013). By reproducing the observed seasonality of atmospheric Hg during 2013–2017 at 44 Northern Hemisphere monitoring sites in model scenarios, the contributions of various meteorological factors to the seasonality were quantified.

2. Methods

2.1. Atmospheric Hg Observations

Atmospheric Hg observations were obtained from monitoring networks located in North America and Europe, including the Canadian Air and Precipitation Monitoring Network (CAPMoN), Atmospheric Mercury Network (AMNet), and European Monitoring and Evaluation Program (EMEP). Additionally, observations in tropical and Asian regions were collected from a literature survey. Observations conducted during 2013–2017 were included in our analysis, and the monthly means were archived for each monitoring site. The Hg^0 species was only recorded at certain monitoring sites, whereas total gaseous mercury (TGM) was widely recorded. For consistency in the present study, TGM was used as a proxy for Hg^0 because it is the dominant component in TGM.

A total of 44 ground-based monitoring sites were included in our analysis because of their multi-year seasonal TGM during 2013–2017. Observations without multi-year seasonal TGM were excluded, although they were collected from the above networks and a literature survey. The monitoring sites were divided into four groups based on their locations, including three temperate Northern Hemisphere groups: North American (NA) remote sites (20 sites), European remote sites (12 sites), Asian monsoon sites (8 sites), and one tropical group (4 sites). The details of the monitoring sites are provided in Table S1 in Supporting Information S1.

2.2. Atmospheric Hg Modeling

The GEOS-Chem chemical transport model (www.geos-chem.org; version 12.5.0) was used to simulate atmospheric Hg cycling and reproduce the observed atmospheric Hg seasonality in the present study. The model is a

global 3-D atmospheric model that includes dynamic coupling between the atmosphere and surface reservoirs for Hg (Amos et al., 2012; Holmes et al., 2010; Horowitz et al., 2017; Selin et al., 2007; Shah et al., 2016). Both Hg⁰ and Hg^{II} are simulated in the model undergoing chemical transformations in the atmosphere and bidirectional transmission between the atmosphere and surface layers. Chemical transformations include the oxidation of Hg⁰ to Hg^{II} by Br and abundant atmospheric radicals (e.g., NO₂ and HO₂), photoreduction of Hg^{II} to Hg⁰ in cloud droplets, and thermodynamic partitioning of Hg^{II} between the gas and particle phases (Amos et al., 2012; Holmes et al., 2010; Horowitz et al., 2017; Shah et al., 2016). Dry deposition follows the standard resistance-in-series scheme (Wesely, 1989), and wet scavenging follows the scheme of Liu et al. (2001), including washout losses in convective updrafts and rainout losses in large-scale precipitation.

Model simulations were driven by assimilated meteorological fields from the NASA Modern-Era Retrospective Analysis for Research and Applications version 2 (MERRA-2) system (Gelaro et al., 2017). All simulations were conducted at 2° latitude × 2.5° longitude resolution and 47 vertical hybrid eta levels from the surface to 0.01 hPa. Four-year simulations were conducted for 2013–2016 with 2013–2014 for initialization and 2015–2016 for analysis. The global anthropogenic emission inventory was derived from Streets et al. (2019), indicating 2.4 Gg yr⁻¹ of Hg was released into the air by human activities in 2015. The model outputs were archived monthly for 2 years on average to reproduce the monthly observations at the monitoring sites.

2.3. Hypothetical Drivers and Model Scenarios

Based on the hypothetical mechanisms previously proposed (Fu et al., 2015; Holmes et al., 2010; Horowitz et al., 2017; Jiskra et al., 2018; Weigelt et al., 2015), both meteorological conditions and other potential drivers, such as vegetation activity, redox fields, biomass burning emissions, and anthropogenic emissions were included in the present study. These drivers would collectively affect atmospheric Hg processes and subsequent Hg seasonality (Figure S1 in Supporting Information S1). For example, vegetation uptake is controlled by vegetation activity, temperature, and solar radiation. It was difficult to enumerate all drivers, however, the representative drivers referenced from previous studies were investigated. These drivers remain relatively independent with meteorological conditions in regard to the direct effects on atmospheric Hg processes. A detailed description of the data sources and seasonal characteristics for these potential drivers, except for meteorological conditions, are provided in Text S1 in Supporting Information S1.

For meteorological conditions, assimilated fields for 2013–2016 were obtained from the NASA MERRA-2 system (Gelaro et al., 2017). The data collection of MERRA-2 has a native resolution of 0.5° latitude × 0.625° longitude with 72 vertical pressure levels and provides us with a complete gridded ensemble of meteorological variables. In addition to the entire meteorological field, seven meteorological factors that can significantly influence atmospheric Hg cycling were tested individually: the height of the planetary boundary layer (PBLH), temperature at 2 m above ground (T2M, namely surface temperature), temperature in the atmospheric vertical columns (T), surface wind at 10 m above ground (UV10M), wind in atmospheric vertical columns (UV), solar radiation, and precipitation. All meteorological factors, including these seven factors, were archived in a 1- or 3-hr time-averaged manner and stored as daily files for the model input. The seasonality of these seven factors in the Northern Hemisphere during 2015–2016 is shown in Figure S2 in Supporting Information S1.

First, a base scenario was run with default model inputs for 2013–2016. The results from the base scenario were used to reproduce the observed seasonality of the TGM concentrations at the monitoring sites. We then ran a model scenario for each driver to individually evaluate the contribution of the specific driver. For each model scenario, the seasonality of the corresponding driver during 2015–2016 was removed by repeating the data in January for the entire year. The contribution of each driver was quantified by comparing the model scenario with the base scenario.

3. Results and Discussion

3.1. Reproducing Observed Atmospheric Hg Seasonality in the Northern Hemisphere

Figures 1a–1h illustrates the distinct seasonality of TGM concentrations at the four studied groups of monitoring sites. The observed seasonality showed lower concentrations during warm months and higher concentrations

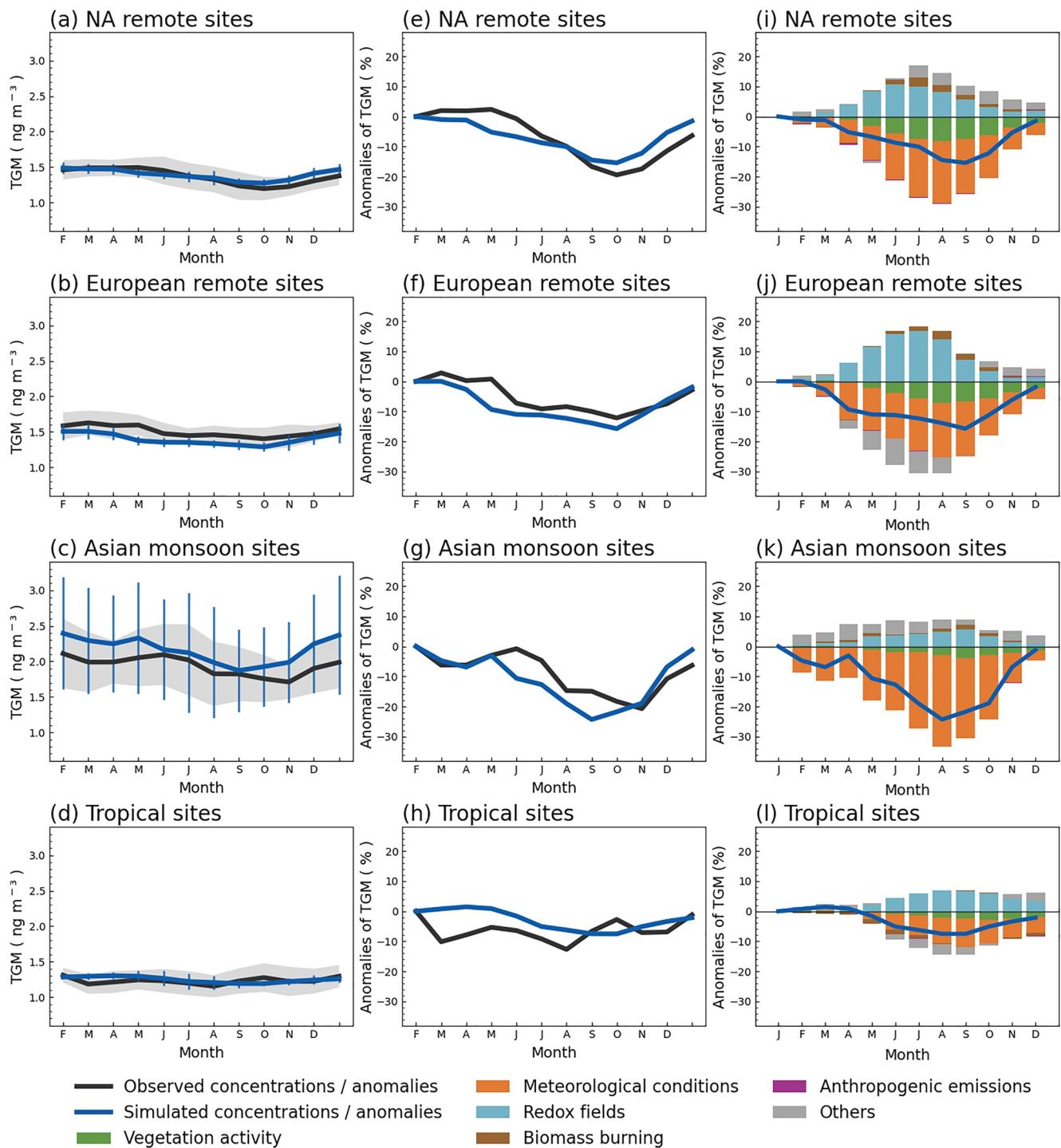


Figure 1. Observed and simulated seasonality of total gaseous mercury (TGM) concentrations (a–h) and contributions of various drivers to the seasonality (i–l) at the Northern Hemisphere sites. The shaded areas and error bars in panels (a–d) represent the standard deviations of observed and simulated concentrations, respectively. Anomalies of TGM concentrations (throughout the text) were calculated through subtracting the absolute value in January from the value in each month and then dividing annual mean.

during cold months at sites in the temperate regions. The anomalies reached negative minima of -19% in September at the NA remote sites, -14% in September at the European remote sites, and -22% in October at the Asian monsoon sites. In contrast, the TGM concentrations at tropical sites showed no significant seasonal oscillations.

Scatter plots correlating the observed annual average TGM concentrations, wet deposition flux, and soil emission flux with the simulations illustrate a good track of the observations obtained by the model (Figures S3 and S4 in Supporting Information S1). The model reproduced TGM seasonality in all the studied groups of monitoring sites (Figures 1a–1h). Good performance was also observed at most of the individual monitoring sites (Figures S5–S8 in Supporting Information S1). Accordingly, the GEOS-Chem model with the latest input data, including meteorological fields and vegetation activity (see Methods), reproduced the observed TGM concentrations and seasonality, laying the foundation for quantifying the contributions of meteorological drivers.

Figures 1i–1l illustrates the contributions of various potential drivers to the observed seasonal anomalies of the TGM concentrations. On average, the combination of these drivers explained approximately 87% of the observed seasonality at all the sites. Meteorological conditions served as the most important drivers of atmospheric Hg seasonality and promoted negative anomalies at all the sites (details in Section 3.2). The negative anomalies driven by meteorological conditions reached negative minima of -21% and -19% at the NA and European remote sites, respectively. On average, throughout the year, the contributions of meteorological conditions can explain approximately 47% and 43% of atmospheric Hg seasonality at the NA and European remote sites, respectively. In addition, high vegetation activity (Figure S9 in Supporting Information S1) contributed to an approximate decrease of -8% during warm months in these two regions, which was attributed to the high stomatal resistance and cuticular resistance of vegetation (Wesely, 1989; Wright & Zhang, 2015). In contrast, the positive anomalies driven by redox fields peaked at 11% and 17% at the NA and European remote sites, respectively, indicating rapid photoreduction of Hg^{II} to Hg^0 in very clean air during warm months in these regions.

Meteorological conditions at the Asian monsoon sites were more important than those at the NA and European remote sites, which contributed to a negative minimum of -32% in August for the negative anomalies, and the contributions of vegetation activity and redox fields were not significant. On average, throughout the year, the contributions of meteorological conditions can explain approximately 67% of atmospheric Hg seasonality at Asian monsoon sites. These inconspicuous contributions were attributed to the profound influence of the typical monsoon climate. Strong monsoon circulation dominates the flow of the Hg-containing air mass, which can weaken the influence of other drivers. Additionally, the low contributions of various drivers were quantified at tropical sites. Weak seasonality of drivers, such as relatively stable meteorological conditions, evergreen forest vegetation, and relatively constant redox fields in the tropics, might account for the weak atmospheric Hg seasonality.

3.2. Evaluating the Indirect Effects of Meteorological Drivers

Based on the key role of meteorological conditions, the contributions of individual meteorological factors that influence atmospheric Hg cycling were evaluated. On average, the combination of seven meteorological factors explained approximately 78% of the total anomalies driven by entire meteorological field (Figure 2).

Similar patterns in the contribution of meteorological factors were observed at the NA and European remote sites. T2M, UV10M, solar radiation, and precipitation were crucial drivers at these sites. The negative anomalies driven by T2M and solar radiation reached negative minima of approximately -12% and -8% at these sites, respectively. High surface temperature and solar radiation can promote the opening of leaf stomata by changing the vapor pressure and photosynthesis-induced water potential of stomatal guard cells, respectively, subsequently increasing Hg assimilation by the leaf mesophyll (Taiz et al., 2014; Wesely, 1989; Wright & Zhang, 2015). Therefore, similar to vegetation activity, increased T2M and solar radiation during warm months (Figures S2b and S2d in Supporting Information S1) also led to a high dry deposition of Hg over the continents (Figures 3e and 3i). Increased solar radiation during warm months also amplifies the photoreduction of Hg compounds in soil and subsequently intensifies soil Hg^0 emissions (Gustin et al., 2002; Lin et al., 2010). However, the potentially increased TGM concentrations driven by enhanced soil emissions were offset by the increased dry deposition, indicating net deposition driven by solar radiation (Figures 3i and 3l). The negative anomalies driven by UV10M reached a negative minimum of approximately -6% at these sites. UV10M mainly participates in oceanic Hg^0 evasion (Nightingale et al., 2000; Soerensen et al., 2010). Low UV10M during warm months (Figure S2e in Supporting Information S1) can reduce the turbulence of surface water and subsequently the frequency of mixing between surface and deep waters, which hinders the supply of Hg substances for reduction from deep water (Soerensen et al., 2013). Consequently, the efficiency of air-sea Hg^0 exchange and related oceanic Hg^0 evasion are reduced. Lower oceanic evasion (Figure 3o) can further decrease TGM concentrations in the marine

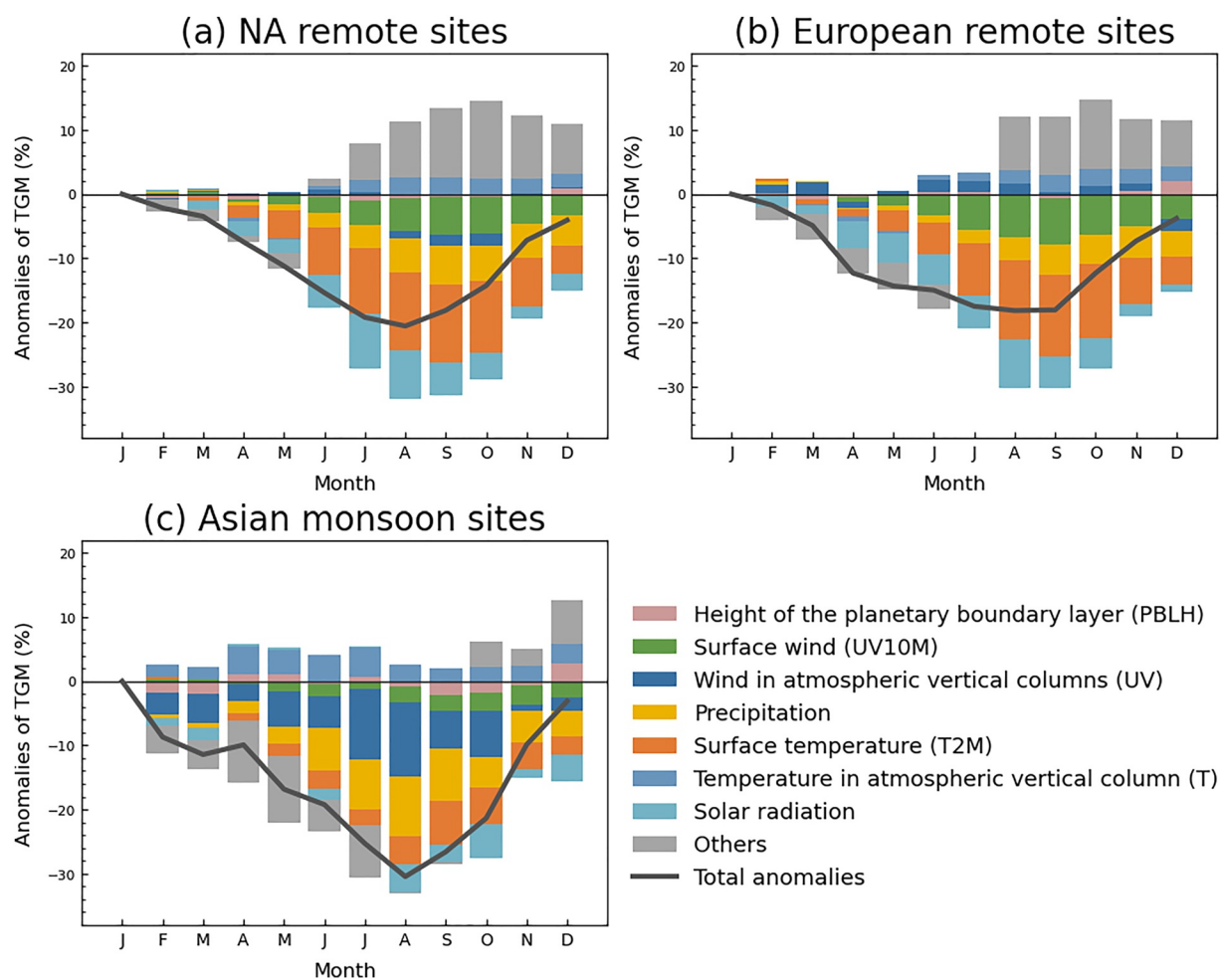


Figure 2. Decomposition of entire meteorological field to individual meteorological factors regarding the anomalies of total gaseous mercury concentrations at the Northern Hemisphere sites. Colored bars and gray line represent the anomalies driven by individual meteorological factors and entire meteorological field, respectively.

boundary layer (MBL) and downwind continents indirectly. Abundant precipitation during the warm months (Figure S2h in Supporting Information S1) enhanced the vertical removal of atmospheric Hg via wet scavenging (Figure 3r), resulting in a negative minimum of approximately -5% at these sites. Other factors, such as PBLH, UV, and T, had relatively small influences on seasonality.

Unlike the NA and European remote sites, UV and precipitation were the dominant contributors at the Asian monsoon sites. The negative anomalies driven by UV and precipitation reached negative minima of approximately -15% and -9% , respectively. The Asian monsoon system is one of the most typical monsoon climate systems worldwide (An et al., 2015), and profoundly influences atmospheric pollutants in Asian monsoon regions (Chen et al., 2020). During warm months, the prevailing south-easterly monsoon wind carried clean air with lower Hg concentrations from the ocean, replacing air with higher Hg concentrations over continental regions (Figure S2g in Supporting Information S1). A significant quantity of water vapor comes from the ocean with the summer monsoon wind, resulting in more precipitation during warm months over the Asian monsoon regions, further enhancing the removal of atmospheric Hg (Liu et al., 2016; Tseng et al., 2012; Yu et al., 2015). Thus, more significant anomalies contributed by precipitation were observed at the Asian monsoon sites than at other temperate sites.

In summary, the typical monsoon climate in Asia leads to differences in the crucial meteorological drivers between the Asian monsoon sites and other monitoring sites in the temperate Northern Hemisphere. Meteorological factors such as UV and precipitation indirectly induced atmospheric Hg seasonality through atmospheric

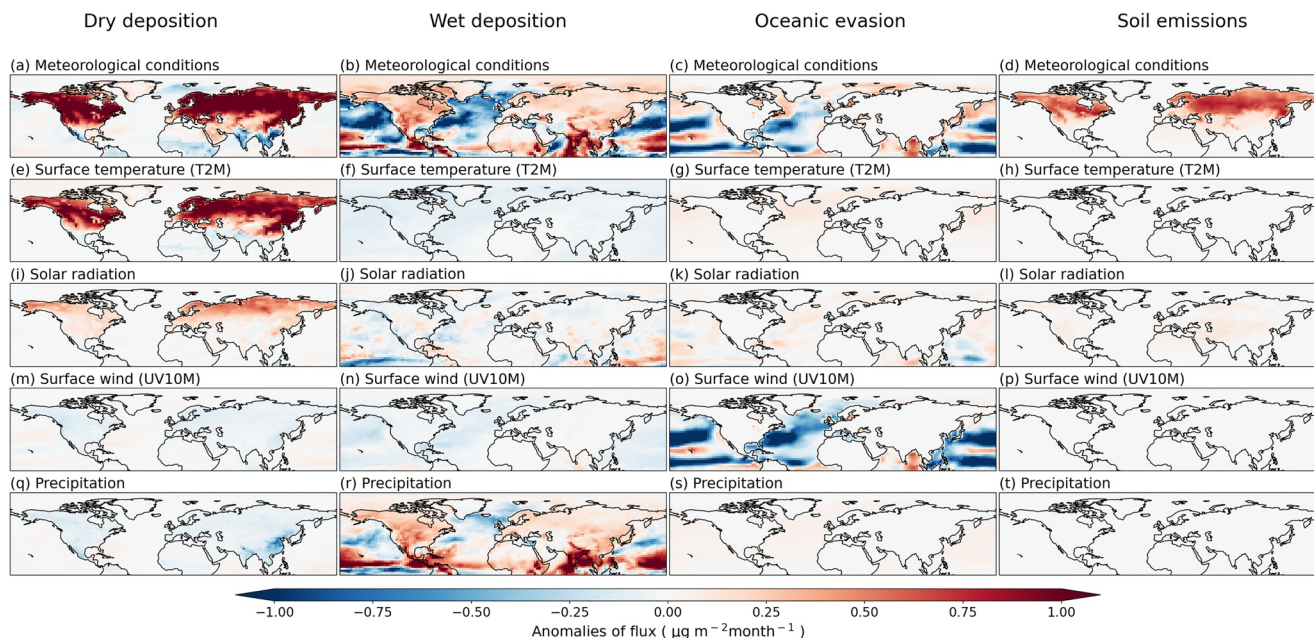


Figure 3. Anomalies of flux in typical atmospheric processes for warm months (July to October) in the Northern Hemisphere driven by entire meteorological field and specific meteorological factors. Panels in a column illustrate a type of atmospheric processes, and the average of anomalies during the 4 months was archived.

transport and wet deposition, and meteorological factors such as T2M, solar radiation, and UV10M indirectly induced atmospheric Hg seasonality through stomatal resistance, soil emissions, and oceanic evasion.

3.3. Mapping the Spatial Distribution of Atmospheric Hg Seasonality

Simulation of the global spatial distribution of surface TGM concentrations using the GEOS-Chem model enabled the presentation of atmospheric Hg seasonality from ground-based monitoring sites to the surface of the Earth, helping to illustrate atmospheric Hg seasonality over regions without Hg observations (Figure 4). Figure 4a shows that the seasonal hotspots of surface TGM concentrations during warm months were located in North America, Europe, North Asia, the Asian monsoon regions, and Central Africa. Meteorological conditions were important drivers of the observed negative anomalies during warm months (Figure 4b), with T2M, solar radiation, and UV10M promoting stomatal uptake and reducing oceanic Hg⁰ evasion in the summer in the Northern Hemisphere, while the monsoon wind and precipitation promoted Hg removal via atmospheric transport and wet deposition in Asia. Owing to the vegetation-induced dry deposition mechanism (Wesely, 1989; Wright & Zhang, 2015), the seasonality of T2M and solar radiation mainly contributed to negative anomalies over the continents (Figures 4d and 4f). The hotspots of negative anomalies were concentrated in regions with dense vegetation, such as Canada, Russia, and Northern Europe. Positive anomalies for solar radiation were observed over certain Asian areas (Figure 4f), which was attributable to the predominant effects of soil emissions driven by solar radiation on land with sparse vegetation (Figures 3i and 3l).

UV mainly contributed to the decrease in surface TGM concentrations during warm months over the Asian monsoon regions, including Southeast Asia, South Asia, the Northwest Pacific, and the northern Indian Ocean (Figure 4h). Conversely, the surface TGM concentrations during warm months significantly increased over inland China and Mongolia. This increase was mainly attributed to the transport of an Hg-containing air mass from the industrialized regions in East China to the northwestern regions with south-easterly monsoon wind (Fu et al., 2015). UV10M mainly contributed to the decrease in surface TGM concentrations in the MBL and downwind continents, including hotspots over the North Pacific, North Atlantic, North America, and Western Europe (Figure 4g). Therefore, UV10M is a crucial driver of atmospheric Hg seasonality at the NA and European remote sites (Figure 2). Precipitation induced a decrease in surface TGM concentrations across the hemisphere, with hotspots in East Asia, South Asia, and the Northwest Pacific (Figure 4i). The hotspots were consistent with the

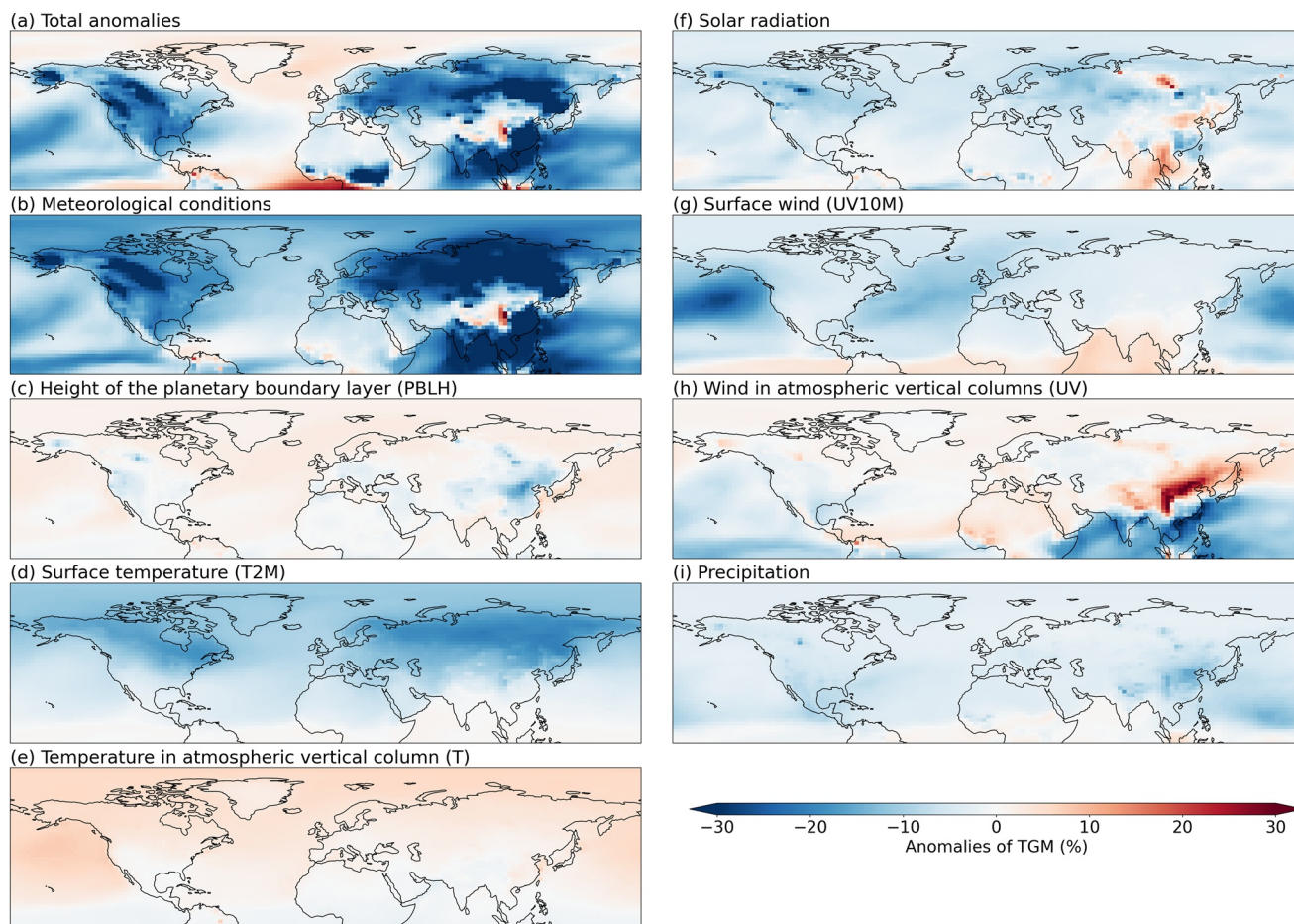


Figure 4. Anomalies of simulated surface total gaseous mercury concentrations for warm months (July to October) in the Northern Hemisphere and contributions of various meteorological factors.

Asian monsoon regions, indicating the important role of monsoon precipitation, which has significant seasonal variability.

4. Implications and Conclusions

Meteorological conditions contributed significantly to atmospheric Hg seasonality, indicating the predictive changes in seasonality in the context of future climate change. Human influence has warmed the climate at an unprecedented rate over the past hundred years, and future greenhouse gas emissions will cause additional warming under various scenarios of Shared Socioeconomic Pathways (IPCC, 2021). The increase in air temperature, particularly surface temperature, will further intensify the stomatal resistance (i.e., stomatal uptake) of vegetation and subsequent dry deposition of Hg. Climate warming can also cause future forest fires and vegetation deaths (Duane et al., 2021; Goss et al., 2020; Ma et al., 2015), resulting in an opposite pattern of stomatal resistance and dry deposition of Hg. Accordingly, uncertainties in the impacts of climate warming have led to uncertainties in projections of future atmospheric Hg seasonality. Precipitation during warm months is projected to increase over high latitudes, the equatorial Pacific, and parts of the monsoon regions due to the increase in moisture flux convergence and local surface evaporation under global warming (IPCC, 2021). These regions coincide with regions where strong atmospheric Hg seasonality exists, indicating likely further strengthened amplitudes of atmospheric Hg seasonality via intensified wet deposition by precipitation.

Based on the above findings, changes in the Asian monsoon system under climate change are expected to significantly influence atmospheric Hg seasonality in the Asian monsoon regions. Land warming over the Eurasian continent is projected because of the increased CO₂ radiative forcing and decreased aerosol cooling effect during

the 21st century, intensifying the land-sea thermal contrast (Endo et al., 2018; Tian et al., 2019; Wang, Zhang, & Zhang, 2016). Consequently, the amplified land-sea thermal contrast can potentially strengthen the circulation and increase the precipitation of the Asian monsoon system. Climate models also project an increase in the length of the summer monsoon season owing to early onset and late retreat (Ha et al., 2020). Amplified monsoon circulation and precipitation and longer monsoon seasons are likely to strengthen future atmospheric Hg seasonality in the Asian monsoon regions. However, a weakening tendency of the Asian monsoon circulation is also projected in several climate models owing to pronounced warming in the mid-to-upper troposphere over the tropics with global warming (Kitoh et al., 2013; Ueda et al., 2006). Thus, significant uncertainties exist in the projections of climate systems such as the Asian monsoon system, resulting in uncertainties in the projections of atmospheric Hg seasonality under future climate change.

To be concluded, meteorological conditions can promote the variations of atmospheric processes which control global Hg cycling, and further indirectly induce atmospheric Hg seasonality across diverse temperate regions in the Northern Hemisphere. Typical monsoon climate in Asia led to differences in effects of meteorological factors from other regions. The findings help both the understanding of driving forces of atmospheric Hg seasonality and future projections of changes in biogeochemical Hg cycles.

Conflict of Interest

The authors declare no conflicts of interest relevant to this study.

Data Availability Statement

Hg observations from the CAPMoN, AMNet, and EMEP are accessible at <https://donnees.ec.gc.ca/data/air/monitor/monitoring-of-atmospheric-gases/total-gaseous-mercury-tgm>, <http://nadp2.slh.wisc.edu/data/AMNet>, and <https://ebas-data.nilu.no>, respectively. Supporting data of the GEOS-Chem model can be obtained at <https://geos-chem.readthedocs.io/en/latest/gcc-guide/04-data/download-data.html>. MERRA-2 reanalysis data is accessible at https://gmao.gsfc.nasa.gov/reanalysis/MERRA-2/data_access. GFED4 data is accessible at <https://www.geo.vu.nl/~gwerf/GFED/GFED4>.

References

- Amos, H. M., Jacob, D. J., Holmes, C. D., Fisher, J. A., Wang, Q., Yantosca, R. M., et al. (2012). Gas-particle partitioning of atmospheric Hg(II) and its effect on global mercury deposition. *Atmospheric Chemistry and Physics*, 12(1), 591–603. <https://doi.org/10.5194/acp-12-591-2012>
- An, Z. S., Wu, G. X., Li, J. P., Sun, Y. B., Liu, Y. M., Zhou, W. J., et al. (2015). Global monsoon dynamics and climate change. *Annual Review of Earth and Planetary Sciences*, 43(1), 29–77. <https://doi.org/10.1146/annurev-earth-060313-054623>
- Aspmo, K., Temme, C., Berg, T., Ferrari, C., Gauchard, P.-A., Fain, X., & Wibetoe, G. (2006). Mercury in the atmosphere, snow and melt water ponds in the North Atlantic Ocean during Arctic summer. *Environmental Science and Technology*, 40(13), 4083–4089. <https://doi.org/10.1021/es052117z>
- Carbone, F., Landis, M. S., Gencarelli, C. N., Naccarato, A., Sprovieri, F., De Simone, F., et al. (2016). Sea surface temperature variation linked to elemental mercury concentrations measured on Mauna Loa. *Geophysical Research Letters*, 43(14), 7751–7757. <https://doi.org/10.1002/2016gl069252>
- Chen, Z., Chen, D., Zhao, C., Kwan, M. P., Cai, J., Zhuang, Y., et al. (2020). Influence of meteorological conditions on PM_{2.5} concentrations across China: A review of methodology and mechanism. *Environment International*, 139, 105558. <https://doi.org/10.1016/j.envint.2020.105558>
- Duane, A., Castellnou, M., & Brotons, L. (2021). Towards a comprehensive look at global drivers of novel extreme wildfire events. *Climatic Change*, 165(3–4), 094016. <https://doi.org/10.1007/s10584-021-03066-4>
- Endo, H., Kitoh, A., & Ueda, H. (2018). A unique feature of the Asian summer monsoon response to global warming: The role of different land-sea thermal contrast change between the lower and upper troposphere. *Sola*, 14(0), 57–63. <https://doi.org/10.2151/sola.2018-010>
- Fu, X., Zhang, H., Liu, C., Zhang, H., Lin, C. J., & Feng, X. (2019). Significant seasonal variations in isotopic composition of atmospheric total gaseous mercury at forest sites in China caused by vegetation and mercury sources. *Environmental Science and Technology*, 53(23), 13748–13756. <https://doi.org/10.1021/acs.est.9b05016>
- Fu, X., Zhang, H., Yu, B., Wang, X., Lin, C. J., & Feng, X. (2015). Observations of atmospheric mercury in China: A critical review. *Atmospheric Chemistry and Physics*, 15(16), 9455–9476. <https://doi.org/10.5194/acp-15-9455-2015>
- Gelaro, R., McCarty, W., Suarez, M. J., Todling, R., Molod, A., Takacs, L., et al. (2017). The modern-era retrospective analysis for research and applications, version 2 (MERRA-2). *Journal of Climate*, 30(14), 5419–5454. <https://doi.org/10.1175/jcli-d-16-0758.1>
- Goss, M., Swain, D. L., Abatzoglou, J. T., Sarhadi, A., Kolden, C. A., Williams, A. P., & Duffenbaugh, N. S. (2020). Climate change is increasing the likelihood of extreme autumn wildfire conditions across California. *Environmental Research Letters*, 15(9), 43. <https://doi.org/10.1088/1748-9326/ab83a7>
- Gustin, M. S., Biester, H., & Kim, C. S. (2002). Investigation of the light-enhanced emission of mercury from naturally enriched substrates. *Atmospheric Environment*, 36(20), 3241–3254. [https://doi.org/10.1016/s1352-2310\(02\)00329-1](https://doi.org/10.1016/s1352-2310(02)00329-1)
- Gustin, M. S., Lindberg, S. E., & Weisberg, P. J. (2008). An update on the natural sources and sinks of atmospheric mercury. *Applied Geochemistry*, 23(3), 482–493. <https://doi.org/10.1016/j.apgeochem.2007.12.010>

Acknowledgments

This study was funded by the National Natural Science Foundation of China (42077200, 41977311, 42125102). The computation was supported by the ECNU Public Platform for Innovation (001).

- Ha, K.-J., Moon, S., Timmermann, A., & Kim, D. (2020). Future changes of summer monsoon characteristics and evaporative demand over Asia in CMIP6 simulations. *Geophysical Research Letters*, *47*(8), 1–10. <https://doi.org/10.1029/2020gl087492>
- Holmes, C. D., Jacob, D. J., Corbitt, E. S., Mao, J., Yang, X., Talbot, R., & Slemr, F. (2010). Global atmospheric model for mercury including oxidation by bromine atoms. *Atmospheric Chemistry and Physics*, *10*(24), 12037–12057. <https://doi.org/10.5194/acp-10-12037-2010>
- Horowitz, H. M., Jacob, D. J., Zhang, Y., Dibble, T. S., Slemr, F., Amos, H. M., et al. (2017). A new mechanism for atmospheric mercury redox chemistry: Implications for the global mercury budget. *Atmospheric Chemistry and Physics*, *17*(10), 6353–6371. <https://doi.org/10.5194/acp-17-6353-2017>
- IPCC. (2021). AR6 climate change 2021: The physical science basis. Retrieved from <https://www.ipcc.ch/report/ar6/wg1/>
- Jiskra, M., Sonke, J. E., Obrist, D., Bieser, J., Ebinghaus, R., Myhre, C. L., et al. (2018). A vegetation control on seasonal variations in global atmospheric mercury concentrations. *Nature Geoscience*, *11*(4), 244–250. <https://doi.org/10.1038/s41561-018-0078-8>
- Kitoh, A., Endo, H., Kumar, K. K., Cavalcanti, I. F. A., Goswami, P., & Zhou, T. J. (2013). Monsoons in a changing world: A regional perspective in a global context. *Journal of Geophysical Research: Atmospheres*, *118*(8), 3053–3065. <https://doi.org/10.1002/jgrd.50258>
- Koenig, A. M., Magand, O., Laj, P., Andrade, M., Moreno, I., Velarde, F., et al. (2021). Seasonal patterns of atmospheric mercury in tropical South America as inferred by a continuous total gaseous mercury record at Chacaltaya station (5240 m) in Bolivia. *Atmospheric Chemistry and Physics*, *21*(5), 3447–3472. <https://doi.org/10.5194/acp-21-3447-2021>
- Krabbenhoft, D. P., & Sunderland, E. M. (2013). Global change and mercury. *Science*, *341*(6153), 1457–1458. <https://doi.org/10.1126/science.1242838>
- Lin, C. J., Gustin, M. S., Singhasuk, P., Eckley, C., & Miller, M. (2010). Empirical models for estimating mercury flux from soils. *Environmental Science and Technology*, *44*(22), 8522–8528. <https://doi.org/10.1021/es1021735>
- Lindberg, S. E., & Stratton, W. J. (1998). Atmospheric mercury speciation: Concentrations and behavior of reactive gaseous mercury in ambient air. *Environmental Science and Technology*, *32*(1), 49–57. <https://doi.org/10.1021/es970546u>
- Liu, H. Y., Jacob, D. J., Bey, I., & Yantosca, R. M. (2001). Constraints from Pb-210 and Be-7 on wet deposition and transport in a global three-dimensional chemical tracer model driven by assimilated meteorological fields. *Journal of Geophysical Research*, *106*(D11), 12109–12128. <https://doi.org/10.1029/2000jd900839>
- Liu, J. J., Wang, L., Zhu, Y., Lin, C. J., Jang, C., Wang, S. X., et al. (2019). Source attribution for mercury deposition with an updated atmospheric mercury emission inventory in the Pearl River Delta Region, China. *Frontiers of Environmental Science & Engineering*, *13*(1), 2. <https://doi.org/10.1007/s11783-019-1087-6>
- Liu, M., Chen, L., Xie, D., Sun, J., He, Q., Cai, L., et al. (2016). Monsoon-driven transport of atmospheric mercury to the South China Sea from the Chinese mainland and Southeast Asia—observation of gaseous elemental mercury at a background station in South China. *Environmental Science and Pollution Research*, *23*(21), 21631–21640. <https://doi.org/10.1007/s11356-016-7432-4>
- Liu, Y., Lin, C.-J., Yuan, W., Lu, Z., & Feng, X. (2021). Translocation and distribution of mercury in biomasses from subtropical forest ecosystems: Evidence from stable mercury isotopes. *Acta Geochimica*, *40*(1), 42–50. <https://doi.org/10.1007/s11631-020-00441-3>
- Lyman, S. N., Cheng, I., Gratz, L. E., Weiss-Penzias, P., & Zhang, L. M. (2020). An updated review of atmospheric mercury. *Science of the Total Environment*, *707*, 135575. <https://doi.org/10.1016/j.scitotenv.2019.135575>
- Ma, X. L., Huete, A., Moran, S., Ponce-Campos, G., & Eamus, D. (2015). Abrupt shifts in phenology and vegetation productivity under climate extremes. *Journal of Geophysical Research: Biogeosciences*, *120*(10), 2036–2052. <https://doi.org/10.1002/2015jg003144>
- MacSween, K., Edwards, G. C., & Beggs, P. J. (2020). Seasonal gaseous elemental mercury fluxes at a terrestrial background site in south-eastern Australia. *Elementa—Science of the Anthropocene*, *8*, 27. <https://doi.org/10.1525/elementa.423>
- MacSween, K., Edwards, G. C., & Howard, D. A. (2020). Up-scaling mercury emissions from terrestrial surfaces as a response to sustained temperature increase. *Atmospheric Environment*, *223*, 117190. <https://doi.org/10.1016/j.atmosenv.2020.117190>
- Nightingale, P. D., Malin, G., Law, C. S., Watson, A. J., Liss, P. S., Liddicoat, M. I., et al. (2000). In situ evaluation of air-sea gas exchange parameterizations using novel conservative and volatile tracers. *Global Biogeochemical Cycles*, *14*(1), 373–387. <https://doi.org/10.1029/1999gb900091>
- Obrist, D., Roy, E. M., Harrison, J. L., Kwong, C. F., Munger, J. W., Moosmuller, H., et al. (2021). Previously unaccounted atmospheric mercury deposition in a midlatitude deciduous forest. *Proceedings of the National Academy of Sciences of the United States of America*, *118*(29), e2105477118. <https://doi.org/10.1073/pnas.2105477118>
- Obrist, D., Tas, E., Peleg, M., Matveev, V., Fain, X., Asaf, D., & Luria, M. (2011). Bromine-induced oxidation of mercury in the mid-latitude atmosphere. *Nature Geoscience*, *4*(1), 22–26. <https://doi.org/10.1038/ngeo1018>
- Pal, B., & Ariya, P. A. (2004). Gas-phase HO center dot-initiated reactions of elemental mercury: Kinetics, product studies, and atmospheric implications. *Environmental Science and Technology*, *38*(21), 5555–5566. <https://doi.org/10.1021/es0494353>
- Roman, H. A., Walsh, T. L., Coull, B. A., Dewailly, E., Guallar, E., Hattis, D., et al. (2011). Evaluation of the cardiovascular effects of methylmercury exposures: Current evidence supports development of a dose-response function for regulatory benefits analysis. *Environmental Health Perspectives*, *119*(5), 607–614. <https://doi.org/10.1289/ehp.1003012>
- Saiz-Lopez, A., Sitkiewicz, S. P., Roca-Sanjuan, D., Oliva-Enrich, J. M., Davalos, J. Z., Notario, R., et al. (2018). Photoreduction of gaseous oxidized mercury changes global atmospheric mercury speciation, transport and deposition. *Nature Communications*, *9*(1), 4796. <https://doi.org/10.1038/s41467-018-07075-3>
- Selin, N. E., Javob, D. J., Park, R. J., Yantosca, R. M., Strobe, S., Jaeglé, L., & Jaffe, D. (2007). Chemical cycling and deposition of atmospheric mercury: Global constraints from observations. *Journal of Geophysical Research*, *112*(2), D02308. <https://doi.org/10.1029/2006JD007450>
- Shah, V., Jaegle, L., Gratz, L. E., Ambrose, J. L., Jaffe, D. A., Selin, N. E., et al. (2016). Origin of oxidized mercury in the summertime free troposphere over the southeastern US. *Atmospheric Chemistry and Physics*, *16*(3), 1511–1530. <https://doi.org/10.5194/acp-16-1511-2016>
- Soerensen, A. L., Mason, R. P., Balcom, P. H., & Sunderland, E. M. (2013). Drivers of surface ocean mercury concentrations and air-sea exchange in the West Atlantic Ocean. *Environmental Science and Technology*, *47*(14), 7757–7765. <https://doi.org/10.1021/es401354q>
- Soerensen, A. L., Sunderland, E. M., Holmes, C. D., Jacob, D. J., Yantosca, R. M., Skov, H., et al. (2010). An improved global model for air-sea exchange of mercury: High concentrations over the North Atlantic. *Environmental Science and Technology*, *44*(22), 8574–8580. <https://doi.org/10.1021/es102032g>
- Sommar, J., Osterwalder, S., & Zhu, W. (2020). Recent advances in understanding and measurement of Hg in the environment: Surface-atmosphere exchange of gaseous elemental mercury (Hg⁰). *Science of the Total Environment*, *721*, 137648. <https://doi.org/10.1016/j.scitotenv.2020.137648>
- Sprovieri, F., Pirrone, N., Bencardino, M., D'Amore, F., Angot, H., Barbante, C., et al. (2017). Five-year records of mercury wet deposition flux at GMOS sites in the Northern and Southern hemispheres. *Atmospheric Chemistry and Physics*, *17*(4), 2689–2708. <https://doi.org/10.5194/acp-17-2689-2017>
- Sprovieri, F., Pirrone, N., Bencardino, M., D'Amore, F., Carbone, F., Cinnirella, S., et al. (2016). Atmospheric mercury concentrations observed at ground-based monitoring sites globally distributed in the framework of the GMOS network. *Atmospheric Chemistry and Physics*, *16*(18), 11915–11935. <https://doi.org/10.5194/acp-16-11915-2016>

- Streets, D. G., Horowitz, H. M., Lu, Z., Levin, L., Thackray, C. P., & Sunderland, E. M. (2019). Global and regional trends in mercury emissions and concentrations. *Atmospheric Environment*, *201*, 417–427. <https://doi.org/10.1016/j.atmosenv.2018.12.031>
- Taiz, L., Zeiger, E., Moller, I. M., & Murphy, A. (Eds.). (2014). *Photosynthesis: Physiological and ecological considerations, stomatal biology, Plant physiology and development* (6 ed., pp. 245–284). Sinauer Associates.
- Temme, C., Blanchard, P., Steffen, A., Banic, C., Beauchamp, S., Poissant, L., et al. (2007). Trend, seasonal and multivariate analysis study of total gaseous mercury data from the Canadian atmospheric mercury measurement network (CAMNet). *Atmospheric Environment*, *41*(26), 5423–5441. <https://doi.org/10.1016/j.atmosenv.2007.02.021>
- Tian, F., Dong, B., Robson, J., Sutton, R., & Tett, S. F. B. (2019). Projected near term changes in the East Asian summer monsoon and its uncertainty. *Environmental Research Letters*, *14*(8), 084038. <https://doi.org/10.1088/1748-9326/ab28a6>
- Tseng, C. M., Liu, C. S., & Lamborg, C. (2012). Seasonal changes in gaseous elemental mercury in relation to monsoon cycling over the northern South China Sea. *Atmospheric Chemistry and Physics*, *12*(16), 7341–7350. <https://doi.org/10.5194/acp-12-7341-2012>
- Ueda, H., Iwai, A., Kuwako, K., & Hori, M. E. (2006). Impact of anthropogenic forcing on the Asian summer monsoon as simulated by eight GCMs. *Geophysical Research Letters*, *33*(6), L06703. <https://doi.org/10.1029/2005gl025336>
- Wang, C., Wang, Z., & Zhang, X. (2020). Characteristics of the air-sea exchange of gaseous mercury and deposition flux of atmospheric mercury at an island near the boundary of the Bohai Sea and Yellow Sea. *Atmospheric Environment*, *232*, 117547. <https://doi.org/10.1016/j.atmosenv.2020.117547>
- Wang, X., Bao, Z., Lin, C.-J., Yuan, W., & Feng, X. (2016). Assessment of global mercury deposition through litterfall. *Environmental Science and Technology*, *50*(16), 8548–8557. <https://doi.org/10.1021/acs.est.5b06351>
- Wang, X., Lin, C. J., Feng, X. B., Yuan, W., Fu, X. W., Zhang, H., et al. (2018). Assessment of regional mercury deposition and emission outflow in mainland China. *Journal of Geophysical Research: Atmospheres*, *123*(17), 9868–9890. <https://doi.org/10.1029/2018jd028350>
- Wang, X., Yuan, W., Lin, C. J., Luo, J., Wang, F., Feng, X., et al. (2020). Underestimated sink of atmospheric mercury in a deglaciated forest chronosequence. *Environmental Science and Technology*, *54*(13), 8083–8093. <https://doi.org/10.1021/acs.est.0c01667>
- Wang, Z. L., Zhang, H., & Zhang, X. Y. (2016). Projected response of East Asian summer monsoon system to future reductions in emissions of anthropogenic aerosols and their precursors. *Climate Dynamics*, *47*(5–6), 1455–1468. <https://doi.org/10.1007/s00382-015-2912-7>
- Weigelt, A., Ebinghaus, R., Manning, A. J., Derwent, R. G., Simmonds, P. G., Spain, T. G., et al. (2015). Analysis and interpretation of 18 years of mercury observations since 1996 at Mace Head, Ireland. *Atmospheric Environment*, *100*, 85–93. <https://doi.org/10.1016/j.atmosenv.2014.10.050>
- Wesely, M. L. (1989). Parameterization of surface resistances to gaseous dry deposition in regional-scale numerical models. *Atmospheric Environment*, *23*(6), 1293–1304. [https://doi.org/10.1016/0004-6981\(89\)90153-4](https://doi.org/10.1016/0004-6981(89)90153-4)
- Wright, L. P., & Zhang, L. (2015). An approach estimating bidirectional air-surface exchange for gaseous elemental mercury at AMNet sites. *Journal of Advances in Modeling Earth Systems*, *7*(1), 35–49. <https://doi.org/10.1002/2014ms000367>
- Wright, L. P., Zhang, L., & Marsik, F. J. (2016). Overview of mercury dry deposition, litterfall, and throughfall studies. *Atmospheric Chemistry and Physics*, *16*(21), 13399–13416. <https://doi.org/10.5194/acp-16-13399-2016>
- Yu, B., Wang, X., Lin, C. J., Fu, X. W., Zhang, H., Shang, L. H., & Feng, X. B. (2015). Characteristics and potential sources of atmospheric mercury at a subtropical near-coastal site in East China. *Journal of Geophysical Research-Atmospheres*, *120*(16), 8563–8574. <https://doi.org/10.1002/2015jd023425>
- Yu, Q., Luo, Y., Wang, S., Wang, Z., Hao, J., & Duan, L. (2018). Gaseous elemental mercury (GEM) fluxes over canopy of two typical subtropical forests in south China. *Atmospheric Chemistry and Physics*, *18*(1), 495–509. <https://doi.org/10.5194/acp-18-495-2018>
- Zhang, H., Feng, X. B., Larssen, T., Qiu, G. L., & Vogt, R. D. (2010). In inland China, rice, rather than Gish, is the major pathway for methylmercury exposure. *Environmental Health Perspectives*, *118*(9), 1183–1188. <https://doi.org/10.1289/ehp.1001915>
- Zhang, Y. X., Song, Z. C., Huang, S. J., Zhang, P., Peng, Y. M., Wu, P. P., et al. (2021). Global health effects of future atmospheric mercury emissions. *Nature Communications*, *12*(1), 3035. <https://doi.org/10.1038/s41467-021-23391-7>
- Zhou, J., Obrist, D., Dastoor, A., Jiskra, M., & Ryjkov, A. (2021). Vegetation uptake of mercury and impacts on global cycling. *Nature Reviews Earth & Environment*, *2*(4), 269–284. <https://doi.org/10.1038/s43017-021-00146-y>

References From the Supporting Information

- AMAP/UNEnvironment. (2019). *Technical background report for the global mercury assessment 2018. Arctic monitoring and assessment programme, Oslo*. Norway/UN Environment Programme, Chemicals and Health Branch. Retrieved from <https://www.amap.no/documents/doc/Technical-Background-Report-for-the-Global-Mercury-Assessment-2018/1815>
- Bash, J. O., Carlton, A. G., Hutzell, W. T., & Bullock, O. R., Jr. (2014). Regional air quality model application of the aqueous-phase photo reduction of atmospheric oxidized mercury by dicarboxylic acids. *Atmosphere*, *5*(1), 1–15. <https://doi.org/10.3390/atmos5010001>
- Blackwell, B. D., Driscoll, C. T., Maxwell, J. A., & Holsen, T. M. (2014). Changing climate alters inputs and pathways of mercury deposition to forested ecosystems. *Biogeochemistry*, *119*(1–3), 215–228. <https://doi.org/10.1007/s10533-014-9961-6>
- Blasing, T. J., Broniak, C. T., & Marland, G. (2005). The annual cycle of fossil-fuel carbon dioxide emissions in the United States. *Tellus Series B Chemical and Physical Meteorology*, *57*(2), 107–115. <https://doi.org/10.1111/j.1600-0889.2005.00136.x>
- Choi, H.-D., & Holsen, T. M. (2009). Gaseous mercury fluxes from the forest floor of the Adirondacks. *Environmental Pollution*, *157*(2), 592–600. <https://doi.org/10.1016/j.envpol.2008.08.020>
- Dibble, T. S., Zelle, M. J., & Mao, H. (2012). Thermodynamics of reactions of ClHg and BrHg radicals with atmospherically abundant free radicals. *Atmospheric Chemistry and Physics*, *12*(21), 10271–10279. <https://doi.org/10.5194/acp-12-10271-2012>
- Donohoue, D. L., Bauer, D., Cossairt, B., & Hynes, A. J. (2006). Temperature and pressure dependent rate coefficients for the reaction of Hg with Br and the reaction of Br with Br: A pulsed laser photolysis-pulsed laser induced fluorescence study. *Journal of Physical Chemistry A*, *110*(21), 6623–6632. <https://doi.org/10.1021/jp054688j>
- Ericksen, J. A., Gustin, M. S., Xin, M., Weisberg, P. J., & Fernandez, G. C. J. (2006). Air-soil exchange of mercury from background soils in the United States. *Science of the Total Environment*, *366*(2–3), 851–863. <https://doi.org/10.1016/j.scitotenv.2005.08.019>
- Fu, X. W., Feng, X. B., & Wang, S. F. (2008). Exchange fluxes of Hg between surfaces and atmosphere in the eastern flank of Mount Gongga, Sichuan province, southwestern China. *Journal of Geophysical Research*, *113*(D20), D20306. <https://doi.org/10.1029/2008jd009814>
- Jiao, Y., & Dibble, T. S. (2017). First kinetic study of the atmospherically important reactions BrHg center dot + NO₂ and BrHg center dot + HOO. *Physical Chemistry Chemical Physics*, *19*(3), 1826–1838. <https://doi.org/10.1039/c6cp06276h>

- Kuiken, T., Zhang, H., Gustin, M., & Lindberg, S. (2008). Mercury emission from terrestrial background surfaces in the eastern USA. Part I: Air/surface exchange of mercury within a southeastern deciduous forest (Tennessee) over one year. *Applied Geochemistry*, 23(3), 345–355. <https://doi.org/10.1016/j.apgeochem.2007.12.006>
- Lamsal, L. N., Krotkov, N. A., Celarier, E. A., Swartz, W. H., Pickering, K. E., Bucsela, E. J., et al. (2014). Evaluation of OMI operational standard NO₂ column retrievals using in situ and surface-based NO₂ observations. *Atmospheric Chemistry and Physics*, 14(21), 11587–11609. <https://doi.org/10.5194/acp-14-11587-2014>
- Lin, J., Liu, Z., Zhang, Q., Liu, H., Mao, J., & Zhuang, G. (2012). Modeling uncertainties for tropospheric nitrogen dioxide columns affecting satellite-based inverse modeling of nitrogen oxides emissions. *Atmospheric Chemistry and Physics*, 12(24), 12255–12275. <https://doi.org/10.5194/acp-12-12255-2012>
- Lin, J., Pan, D., Davis, S. J., Zhang, Q., Guan, D., Wang, C., et al. (2014). China's international trade and air pollution in the United States. *Proceedings of the National Academy of Sciences of the United States of America*, 111(5), 1736–1741. <https://doi.org/10.1073/pnas.1312860111>
- Liu, J. J., Wang, L., Zhu, Y., Lin, C. J., Jang, C., Wang, S. X., et al. (2019). Source attribution for mercury deposition with an updated atmospheric mercury emission inventory in the Pearl River Delta Region, China. *Frontiers of Environmental Science & Engineering*, 13(1), 2. <https://doi.org/10.1007/s11783-019-1087-6>
- Liu, K. Y., Wu, Q. R., Wang, L., Wang, S. X., Liu, T. H., Ding, D., et al. (2019). Measure-specific effectiveness of air pollution control on China's atmospheric mercury concentration and deposition during 2013–2017. *Environmental Science and Technology*, 53(15), 8938–8946. <https://doi.org/10.1021/acs.est.9b02428>
- Liu, Y., Liu, R. G., & Chen, J. M. (2012). Retrospective retrieval of long-term consistent global leaf area index (1981–2011) from combined AVHRR and MODIS data. *Journal of Geophysical Research*, 117(G4), G04003. <https://doi.org/10.1029/2012jg002084>
- Ly Sy Phu, N., Zhang, L., Lin, D.-W., Lin, N.-H., & Sheu, G.-R. (2019). Eight-year dry deposition of atmospheric mercury to a tropical high mountain background site downwind of the East Asian continent. *Environmental Pollution*, 255, 113128. <https://doi.org/10.1016/j.envpol.2019.113128>
- Ma, M., Wang, D., Du, H., Sun, T., Zhao, Z., Wang, Y., & Wei, S. (2016). Mercury dynamics and mass balance in a subtropical forest, southwestern China. *Atmospheric Chemistry and Physics*, 16(7), 4529–4537. <https://doi.org/10.5194/acp-16-4529-2016>
- Nie, X., Mao, H., Li, P., Li, T., Zhou, J., Wu, Y., et al. (2020). Total gaseous mercury in a coastal city (Qingdao, China): Influence of sea-land breeze and regional transport. *Atmospheric Environment*, 235, 117633. <https://doi.org/10.1016/j.atmosenv.2020.117633>
- Qin, X., Wang, X., Shi, Y., Yu, G., Zhao, N., Lin, Y., et al. (2019). Characteristics of atmospheric mercury in a suburban area of east China: Sources, formation mechanisms, and regional transport. *Atmospheric Chemistry and Physics*, 19(9), 5923–5940. <https://doi.org/10.5194/acp-19-5923-2019>
- Schmidt, J. A., Jacob, D. J., Horowitz, H. M., Hu, L., Sherwen, T., Evans, M. J., et al. (2016). Modeling the observed tropospheric BrO background: Importance of multiphase chemistry and implications for ozone, OH, and mercury. *Journal of Geophysical Research: Atmospheres*, 121(19), 11819–11835. <https://doi.org/10.1002/2015jd024229>
- Tang, Y., Wang, S., Wu, Q., Liu, K., Wang, L., Li, S., et al. (2018). Recent decrease trend of atmospheric mercury concentrations in East China: The influence of anthropogenic emissions. *Atmospheric Chemistry and Physics*, 18(11), 8279–8291. <https://doi.org/10.5194/acp-18-8279-2018>
- Van der Werf, G. R., Randerson, J. T., Giglio, L., van Leeuwen, T. T., Chen, Y., Rogers, B. M., et al. (2017). Global fire emissions estimates during 1997–2016. *Earth System Science Data*, 9(2), 697–720. <https://doi.org/10.5194/essd-9-697-2017>
- Wang, D. Y., He, L., Shi, X. J., Wei, S. Q., & Feng, X. B. (2006). Release flux of mercury from different environmental surfaces in Chongqing, China. *Chemosphere*, 64(11), 1845–1854. <https://doi.org/10.1016/j.chemosphere.2006.01.054>
- Xiao, Z. Q., Liang, S. L., & Jiang, B. (2017). Evaluation of four long time-series global leaf area index products. *Agricultural and Forest Meteorology*, 246, 218–230. <https://doi.org/10.1016/j.agrformet.2017.06.016>
- Xiao, Z. Q., Liang, S. L., Wang, J. D., Chen, P., Yin, X. J., Zhang, L. Q., & Song, J. L. (2014). Use of general regression neural networks for generating the GLASS leaf area index product from time-series MODIS surface reflectance. *IEEE Transactions on Geoscience and Remote Sensing*, 52(1), 209–223. <https://doi.org/10.1109/tgrs.2013.2237780>
- Xiao, Z. Q., Liang, S. L., Wang, J. D., Xiang, Y., Zhao, X., & Song, J. L. (2016). Long-time-series global land surface satellite leaf area index product derived from MODIS and AVHRR surface reflectance. *IEEE Transactions on Geoscience and Remote Sensing*, 54(9), 5301–5318. <https://doi.org/10.1109/tgrs.2016.2560522>
- Yuan, H., Dai, Y., & Li, S. (2020). *Reprocessed MODIS version 6 leaf area index data sets for land surface and climate modelling*. Sun Yat-sun University. Retrieved from <http://globalchange.bnu.edu.cn/research/lai/v6>
- Yuan, H., Dai, Y. J., Xiao, Z. Q., Ji, D. Y., & Shanguan, W. (2011). Reprocessing the MODIS Leaf Area Index products for land surface and climate modelling. *Remote Sensing of Environment*, 115(5), 1171–1187. <https://doi.org/10.1016/j.rse.2011.01.001>
- Zhu, Z. C., Bi, J., Pan, Y. Z., Ganguly, S., Anav, A., Xu, L., et al. (2013). Global data sets of vegetation leaf area index (LAI)3g and fraction of photosynthetically active radiation (FPAR)3g derived from global inventory modeling and mapping studies (GIMMS) normalized difference vegetation index (NDVI)3g for the period 1981 to 2011. *Remote Sensing*, 5(2), 927–948. <https://doi.org/10.3390/rs5020927>